

Uncovering quantum characteristics of incipient evolutions at the photosynthetic oxygen evolving complex

Pei-Ying Huo,¹ Wei-Zhou Jiang,^{1,*} Rong-Yao Yang,¹ and Xiu-Rong Zhang²

¹*School of Physics, Southeast University, Nanjing 211189, China*

²*School of Science, Jiangsu University of Science and Technology, Zhenjiang 212100, China*

Water oxidation of photosynthesis at the oxygen evolving complex (OEC) is driven by the polarization field induced by the photoelectric hole. By highlighting the role of the polarization field in reshaping the spin and orbit potentials, we reveal in this work the characteristics and underlying mechanism in the relatively simpler OEC evolutions within the states $S_0 \sim S_2$ prior to the water oxidation. The characteristic shifts of the density of states (DOS) of the electron donor Mn atom are observed in the vicinity of the Fermi surface to occur with the spin flips of Mn atoms and the change of the Mn oxidation states during the electron transfer. Notably, the spin flips of Mn atoms point to the resulting spin configuration of the next states. It is found that the electron transfer tend to stabilize the catalyst OEC itself, whereas the proton transfer pushes the evolution forward by preparing a new electron donor, demonstrating the proton-coupled electron transfer. Meanwhile, it shows that the Mn-O bonds around the candidate Mn atom of the electron donor undergo characteristic changes in the bond lengths during the electron transfer. These concomitant phenomena uncovered in first-principle calculations characterize the essential equilibrium of the OEC between the state evolution and stability that forms a ground of the dynamic OEC cycles. In particular, the characteristic undulation of the DOS around the Fermi level occurring at the proton-coupled electron transfer can be used to reveal crucial processes in a wide range of realistic systems.

I. INTRODUCTION

The photosynthesis plays a crucial role in producing the biochemical energy to sustain the Earth's biological cycle. In converting the solar energy into the biochemical energy, the photosystem needs a carousal of electrons eventually from the water oxidation. Water oxidation is thus a fundamental reaction that is catalyzed at the oxygen evolving complex (OEC) in photosystem II (PSII) [1–5]. The whole catalytic process has long been thought to experience five redox reactions in a closed cycle, dubbed Kok's cycle (S_i , $i=0, \dots, 4$) [6], driven by the photoelectric hole at the PSII reaction centre, P_{680} [7], whereas its complete understanding remains challenging and a hot frontier.

In recent decade, the striking advances have arisen mainly from the measurements of the structures of S_i states using the high-resolution X-ray diffraction of the crystalized photosystems since the identification of the S_1 state structure in 2011 [8]. From then on, a series of experiments have progressively performed to identify the structures of S_2 and S_3 states [9–16]. Though the structure of S_4 state remains elusive, latest detection using serial femtosecond X-ray crystallography identified the presence of this intermediate on the time sequence of the evolution [17]. Another annual progress involving the S_4 state and subsequent oxygen radical identification was made strikingly upon the microsecond infrared spectroscopy of various vibration modes of protonated carboxylate sidechains [18]. The two different experiments provide complementary information on the

S_4 state and the mechanism of the O_2 formation, but the characteristic time scale of events remains rather different in these identifications. In addition to the structures of five S_i states, more information is indeed involved in the OEC reactions that include more intermediates associated with redox processes, deprotonations, water insertions and splitting, and the site-directed ionic interactions as well [5, 19].

For the supercomplex system that features multiple intermediates and piecewise evolution processes, in pursuit of simplicity is a natural strategy implemented not only in search of underlying laws but also with appropriately chosen systems. Therefore, this work focuses on the relatively simple evolutions between S_0 and S_2 prior to the water insertion and dissociation. The underlying laws for the evolutions of $S_0 \sim S_2$ can be used to understand the more involved subsequent state evolutions including the pending S_4 state. In particular, the evolutions of $S_0 \rightarrow S_1$ and $S_3 \rightarrow S_4$ are equally characteristic of the transfer of an electron and a proton. The state evolution is primely started by the photoelectric hole that provides a Coulomb attraction to induce a serial electron transfer through the tyrosine residue (Tyr161) [20–22]. Concurrently, the polarization effect arising from the photoelectric hole and transferring electrons modifies the the Coulomb potentials and consequently causes a series of variations in electronic structures. In our previous work, it was found that the spin flips of Mn atoms can serve as a marker under the polarization field to trace the evolving intermediates and OEC states [23]. In light of the spin flips, this work aims to dig out systematically the characteristic signals of the state evolutions under the polarization fields. In particular, we will scrutinize the interplay between the proton and electron transfers during the state evolutions in terms of the characteristic

* wzjiang@seu.edu.cn

signals in the electron density of the states (DOS).

In deed, the relationship between electron and proton transfers during the state evolutions is scarcely elucidated in the literature and remains largely unclear [24–29]. The depth of the recognition about the relationship is restrained by the limited evidences that the Tyr161 deprotonation is followed by a backward proton migration cooperatively with the electron transfer from the CaMn_4O_5 [21, 30, 31], while the proton and electron transfer sequence in the S_2 state seems to rely on the initial open or closed geometry of the S_2 state [23, 30, 32]. These situations lead naturally to the question of how the proton and electron transfers couple in the OEC evolution. Notably, it is known that some redox in the aqueous or hydrogen-rich environments can occur with the proton-coupled electron transfer (PCET). Examples of the PCET range from chemical, catalytic to biological processes, such as enzymatic C-H oxidation [33–35], DNA synthesis and repair [36–38], ribonucleotide reduction [39], and the interconversion reactions of small molecules like $\text{O}_2/\text{H}_2\text{O}$ [40, 41], N_2/NH_3 [42, 43], and $\text{CO}_2/\text{alkanes}$ [44, 45]. In this circumstance, broad significance can be assigned to our study on the characteristic relationship between the electron and proton transfers that is instructive for understanding a variety of processes, say, in catalysis [46, 47], synthetic chemistry [48–50] and energy conversion [51–53], and is of potential applications.

As the evolutions of $S_0 \sim S_2$ are characterized mainly by electron transfers in the redox reactions of the CaMn_4O_5 cluster, concomitant changes are weaved by the shift of the local Coulomb field, the spin flips of Mn atoms, and propagated wrinkles in the electron density of states (DOS) near the Fermi surface. Using the density functional theory, we will search for the characteristic phenomenologies among these changes during the evolutions from S_0 to S_2 through S_1 . We will find that the characteristic phenomenologies can serve as the precursor to reveal the underlying physics of the water oxidation cycle.

II. COMPUTATIONAL METHODS

We perform the spin-polarized all-electron density functional simulations with the DMol³ package in the Materials Studio of Accelrys Inc. The OEC system in the simulation is a 112-atom configuration whose schematic diagram in Fig. 1 is intercepted from the XRD crystal data obtained at 1.9 Å resolution [8]. The prototype of the S_1 state is the 112-atom geometric model, and optimization is performed to obtain the S_1 state structure. The S_0 and S_2 states are the results of optimization, with the prototypes also arising from 112-atom geometric model of the S_1 state by adding back a hydrogen atom and removing an electron, respectively.

In the geometric optimization process, we adopt the B3LYP hybrid functional [54–57] and a double numer-

ical basis set with polarization functions (DNP). The Grimme method for dispersion correction (DFT-D) is applied to account for weak residue interactions. In the self-consistent field (SCF) process, the convergence criterion is set to 1.0×10^{-5} Ha, and the direct inversion in the iterative subspace (DIIS) method is used to accelerate SCF convergence. All eight possible Mn spin configurations ($\uparrow\uparrow\uparrow\uparrow$, $\downarrow\downarrow\downarrow\downarrow$, $\uparrow\downarrow\uparrow\downarrow$, $\uparrow\uparrow\downarrow\downarrow$, $\uparrow\downarrow\downarrow\uparrow$, $\downarrow\uparrow\uparrow\downarrow$, $\downarrow\downarrow\uparrow\uparrow$, $\uparrow\uparrow\downarrow\uparrow$) of the CaMn_4O_5 structure are considered, and the configuration with the lowest energy is identified as the S_1 state structure.

The dynamic process of the electron transfer to the hole at Tyr161 induced by the polarization field is simulated by setting a point charge of the hole with 1.0e at Tyr161 and increasing the equivalent charge of the transferring electron placed at the fixed distance of 2 Å away from Ca atom of CaMn_4O_5 on the line connecting to the O atom of Tyr161. The fractional equivalent charge such as -0.1~ -0.9e is placed to simulate the distance-dependent Coulomb potential in a gradual transfer process of the electron. The effect of the position of the transferring electron is further verified by moving the equivalent charge of -0.9e to the position at a distance of 4 Å away from the Ca atom of CaMn_4O_5 , which is closer to the hole for further hole-electron recombination. With the Coulomb fields of the point charges being included, optimization calculations are performed. In the simulation, the constraint of the charge conservation is imposed on the whole system. More details can be referred to Ref. [23]. Here, modeling the electron transfer by setting the fractional charge can be reasonably simulated by the ab initio molecular dynamics in a time scale of a few hundred of fs [32, 58].

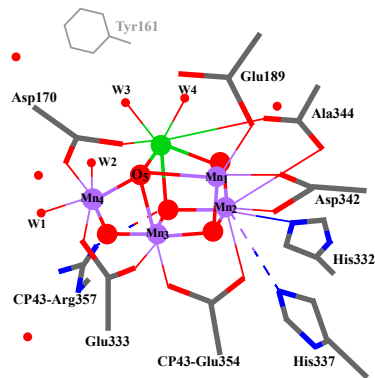


FIG. 1. Geometric model schematic diagram of the OEC CaMn_4O_5 , along with surrounding ligated amino acid residues. Hydrogen atoms are omitted for clarity, while the Tyr161 outside of the model is sketched. The Mn, Ca, and O atoms are represented by solid circles in purple, green, and red colors, respectively. The intersections of the grey, red, and blue solid lines correspond to the ligand C, O, and N atoms, respectively. Single red dots represent water molecules surrounding amino acid residue ligands.

III. RESULTS AND DISCUSSION

The evolutions from S_0 to S_2 primarily involve the transfer of electrons and protons from the CaMn_4O_5 , while the electron transfer fulfills at the hole-electron recombination. The dynamic electron transfer is associated with the variations in the bond valence and polarization field. Hence, elucidating the dynamic electron transfer can detail the animated evolution of CaMn_4O_5 and extract the characteristic phenomena in the presence of the varying polarization field. For $S_0 \sim S_2$ states, the oxidation states of $\text{Mn}_1 \sim \text{Mn}_4$ are reproduced to be S_0 (III, IV, III, III), S_1 (III, IV, IV, III), S_2 -open (III, IV, IV, IV), and S_2 -closed (IV, IV, IV, III), with the spin configurations of $\text{Mn}_1 \sim \text{Mn}_4$ being $\uparrow\downarrow\uparrow\downarrow$, $\uparrow\downarrow\downarrow\uparrow$, $\uparrow\downarrow\downarrow\uparrow$, and $\uparrow\uparrow\uparrow\downarrow$, respectively [1, 59]. Here, the spin configurations are verified to be consistent with those obtained from the complete active space self-consistent field calculation with the explicit inclusion of the spin-orbit coupling [60].

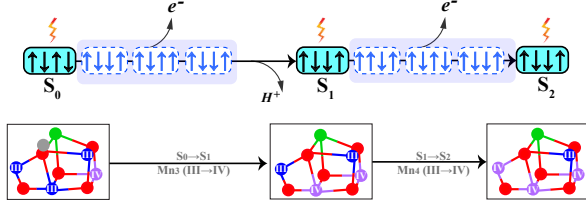


FIG. 2. Evolutions of spin configurations and oxidation states of Mn atoms for $S_0 \sim S_2$. The spins in solid and dashed boxes are for the S_1 and intermediate states, respectively. In the second row, the Mn atoms are marked with oxidation states (III and IV), and Ca, O, and H atoms are denoted by green, red, and grey spheres, respectively.

When the hole polarization field switches on after the oxidation of Tyr161, the Mn spin configuration of the S_0 state flips from $\uparrow\downarrow\uparrow\downarrow$ to $\uparrow\downarrow\downarrow\uparrow$, accompanied by an increase in the total energy of the system. In response to the hole polarization field, the system undergoes an excitation to an intermediate for subsequent electron transfer. The similar spin flip of the S_1 state occurs in the hole polarization field with the Mn spin configuration to $\uparrow\uparrow\uparrow\downarrow$. Then, the candidate Mn atom of the electron donor loses one electron for recombination with the hole at Tyr161.

In the process of the electron transfer from the OEC, the effective charge of the transferring electron is set to vary from -0.1e to -0.9e at a site 2 Å away from the Ca atom of CaMn_4O_5 on the line connecting to the O atom of Tyr161. During this process, we can observe that the spin configuration of Mn atoms undergoes some intermediate configurations and flip exactly to that of the next S state, see Fig. 2. In the evolution from S_0 to S_1 , the Mn spin configuration ultimately changes to $\uparrow\downarrow\downarrow\uparrow$ after going through $\uparrow\downarrow\uparrow\downarrow$. When the released electron moves closer to Tyr161 at a distance of 4 Å away from the Ca atom of the CaMn_4O_5 , the spin configuration of Mn atoms remains unchanged. The subsequent proton removal also

does not alter the Mn spin configuration of $\uparrow\downarrow\downarrow\uparrow$, which then becomes the spin configuration of the S_1 state. Similar spin flips are observed in the process of an electron transfer from the OEC of the S_1 state, as shown in Fig. 2. After the electron transfer, the spin configuration shifts to that of the S_2 -open. Since the occurrence of the spin flips of Mn atoms is attributed to the electron transfer and the resulting shift in the Coulomb field induced by the hole polarization, the spin flips can serve as an indicative marker for the pivotal OEC evolution driven by the hole polarization.

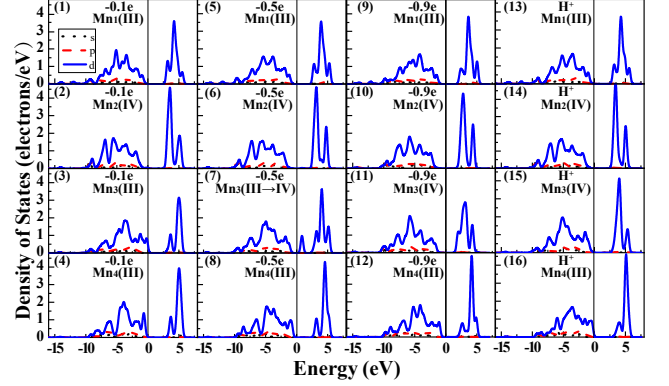


FIG. 3. The PDOS of s, p and d orbitals of $\text{Mn}_1 \sim \text{Mn}_4$ during $S_0 \rightarrow S_1$. Column panels are with effective charge of -0.1, -0.5 and -0.9 e of the transferring electron and with the proton transfer, respectively. The vertical line represents the Fermi surface.

Shown in Fig. 2 is also the variation in the bond valence of Mn atom that represents for an electron transmission from below the Fermi surface to the liberation of the Coulomb binding. This demonstrates the necessity to examine the variation in the density of states (DOS) especially near the Fermi surface in the process of the electron transfer. Figure 3 shows the variation in the partial DOS (PDOS) of s, p and d orbitals for the atoms of $\text{Mn}_1 \sim \text{Mn}_4$ with increasing the effective charge of the transferring electron at the specified position during the evolution from S_0 to S_1 . It is found that in the S_0 state the value of the Mn_3 DOS of the d orbital is significant at the site sufficiently near Fermi surface. We can observe from the third row of Fig. 3 that the Mn_3 DOS of the d orbital comes across the Fermi surface to form a small separate peak that blends into the bumps above the Fermi surface in a process where the electron transfer is simulated by placing the effective charge of -0.1, -0.5 and -0.9e at the site specified above, respectively. Compared with the sluggish changes in the PDOS of other Mn atoms, it clearly suggests that Mn_3 is the electron donor during the evolution from S_0 to S_1 , which is actually in accord with the variation of the Mn oxidation state. During the electron transfer until its fulfillment, the PDOS boundaries of Mn atoms below the Fermi surface experience more or less a contraction inwards to keep the electron distributions better bound. This leads to a temporary

stability of the OEC in the dynamical OEC evolution prior to the proton transfer. The proton transfer pushes the PDOS of Mn atoms outwards and especially brings the Mn₄ PDOS to scrape over the Fermi surface. This gives the opportunity and vigor for another ignition.

As another light flash breaks the tranquility, the photoelectric hole is recreated to drive the evolution from the S₁ to S₂ state. Similar variations in the Mn PDOS arise from the electron transmission from below the Fermi surface. At this time, it is the Mn₄ PDOS that shows the animation from coming across the Fermi surface to undergoing the splitting and blending into high-level distributions well above the Fermi surface, characterizing the Mn₄ oxidation as shown clearly in Fig. 4. Similar to the evolution from the S₀ to S₁ state, the release of electron seems to stabilize the catalyst cluster. This establishes the essential equilibration between the dynamic evolution and the state stability that forms a necessary foundation for the precessing OEC cycle. Moreover, it should be stressed that the electron transfer here is correlated with the preceding proton transfer with which the hydrogen bonding network is associated tightly [61].

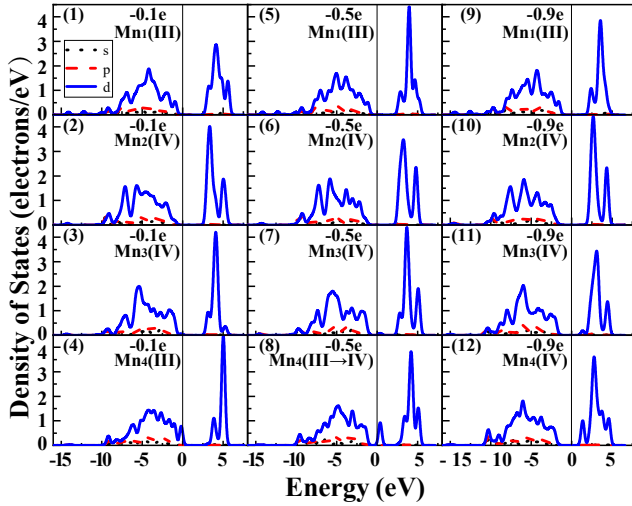


FIG. 4. The same as in Fig. 3 but for S₁→S₂ without proton transfer.

During the electron transfer, the PDOS of all Mn atoms in the Fermi sea is observed to undergo some rearrangements. As a result, the concomitant microscopic changes are also found in the oxidation states and spin configurations of Mn atoms, as shown in Fig. 5. Here, the Mn oxidation state is calculated from the bond valence sum (BVS) formula $S = \sum \exp(R_0 - R_{ij})/B_0$, where R_{ij} represents each bond length between the Mn and surrounding O or N atoms, and other relevant parameters are taken as $B_0=0.37$, $R_0(\text{Mn-O})=1.750$ Å, and $R_0(\text{Mn-N})=1.822$ Å [62]. It can be observed from Fig. 5a and b that the variations in the oxidation states of the candidate Mn atoms of the electron donor are almost linearly correlated with the effective charge of the transferring electron, while the oxidation states of other Mn atoms

remain nearly unchanged. Specifically, with the effective charge of the transferring electron varying from -0.1 to -0.9 e, the Mn₃ oxidation state gradually changes from about 2.9 to 3.7 in S₀→S₁ and Mn₄ changes from 2.8 to 3.7 in S₁→S₂, representing a valence change from III to IV. During the electron transfer in the polarization field, the spin flips of Mn atoms may occur with the changes of Mn oxidation states. Depicted in Fig. 5c and d are the Mulliken spin populations of Mn atoms that give the number of unpaired electrons around Mn and the spin orientations. The positive and negative values correspond to up and down spin orientations, respectively. The reduction of the Mn₃ and Mn₄ spin populations from 4 to 3 in S₀→S₁ and S₁→S₂ accords with the shift of their oxidation states from III to IV for the electron transfer. It can be seen from Fig. 5c and d that some intermediate states are produced with the spin flips of Mn atoms during the electron transfer. Especially, multiple flips of the Mn spin orientations take place in the transfer process of S₁→S₂. With a succession of intermediate states in the varying polarization field, the OEC states (S₀, S₁) evolve to the next state with the electronic and geometric structures consistent with those from the measurements and theoretical computations [63–70].

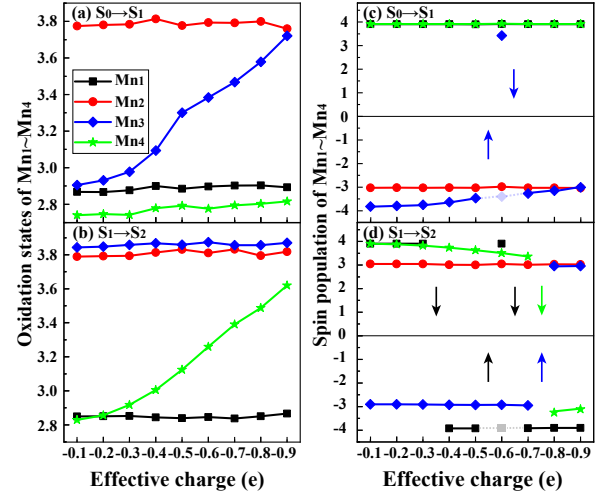


FIG. 5. Variations of Mn₁~Mn₄ oxidation states (a) and (b), and their Mulliken spin population (c) and (d). The effective charge of the transferring electron varies from -0.1 to -0.9 e with the polarization field imposed. The arrows in (c) and (d) represent the flip of spin orientation.

In the dynamical evolution, the above microscopic quantum shifts are also accompanied by the change in the phenomenological geometrical structure. Figure 6 displays the variations of Mn-O₅ and Mn-Mn bond length during the electron transfer under the polarization field. In Fig. 6a and b, the variations of the bond lengths during the electron transfer of S₀→S₁ and S₁→S₂ are relative to those of S₀ and S₁ states, respectively. Positive and negative values stand for the elongation and shortening of bond lengths, respectively. It can be observed that

the alteration in Mn-O bond lengths is more appealing due to the attraction between them, while the less altered Mn-Mn distances suggest that the S_i structures are rather stable during the electron transfer. In Fig. 6a, the main change is observed to be the considerable shortening of the Mn_3-O_5 bond length that is approximately 0.35 \AA with the effective charge of the transferring electron varying from -0.1 to $-0.9 e$ during the electron transfer from S_0 to S_1 state. The large shortening arises from the electron loss of Mn_3 that gives rise to a stronger attraction between Mn_3 and O_5 .

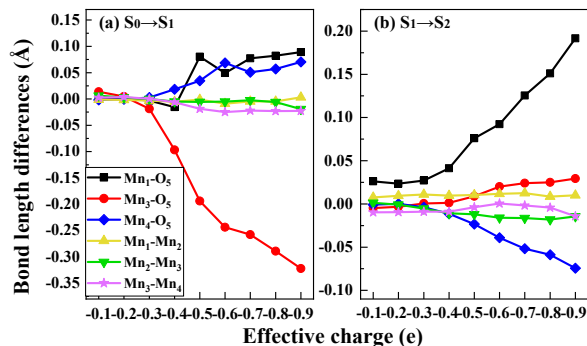


FIG. 6. Variations of Mn- O_5 and Mn-Mn bond lengths. In (a) and (b), the results are relative to those of the S_0 and S_1 states, respectively. The effective charge of the transferring electron varies from -0.1 to $-0.9 e$ with the polarization field imposed.

In the evolution of $S_1 \rightarrow S_2$, the Mn_1-O_5 length shows an overall trend of elongation, while the Mn_4-O_5 length displays the opposite trend of shortening, as the effective charge of the transferring electron varies from -0.1 to $-0.9 e$, see Fig. 5b. The shortening of the Mn_4-O_5 bond length is attributed to the enhanced attraction between Mn_4 and O_5 due to the electron loss of Mn_4 . In contrast, the attraction between Mn_1 and O_5 is weakened to cause the elongation of the bond length. Specifically, the Mn_1-O_5 length increases by about 0.2 \AA throughout the electron transfer process, corresponding to the Mn_1-O_5 bond length of 2.901 and 3.092 \AA in S_1 and S_2 -open state, respectively. The active variation of the Mn_1-O_5 and Mn_4-O_5 bonds suggests the existence of the live domain in the OEC structure. Actually, the counteraction between the Mn_1-O_5 and Mn_4-O_5 bondings offers

support for the existence of two structures that are characteristic of the commodious space with the elongated bond length of Mn_1-O_5 and Mn_4-O_5 , called S_2 -open and S_2 -closed [67], respectively.

IV. SUMMARY

In this work, we investigate the OEC evolutions during $S_0 \sim S_2$ to reveal the animation and mechanisms therein by virtue of the characteristic signals with the density functional simulations. The electron transfer is eventually driven by the hole polarization, whereas a direct evidence of the correlation with the proton transfer is revealed in the state evolution during which the electron donor Mn atom is readily prepared by the preceding proton transfer. The characteristic shift of the Mn PDOS near the Fermi surface is found to correlate simultaneously with the variations in the Mn oxidation states and spin flips, together with the change in the geometric structure. These concurrent events consist of a collection of the characteristic signals for the state evolution. In particular, the spin flips of Mn atoms, consistent with variation of the Mulliken spin populations, can point exactly to the spin configuration of the next S_i state after undergoing some intermediates during electron transfer. Importantly, the stability of the OEC arising from the electron transfer brings the rhythm in the theme of the dynamical evolution that is necessary for the unceasing OEC cycle. Our findings will play an instructive role in unveiling the pending S_4 state and revealing more underlying physics for the water oxidation cycle. Moreover, the direct evidence of the correlation of the proton and electron transfers in the PDOS on the Fermi energy level can be instructively used as a tracer to tag and understand a wide range of biochemical processes and redox reactions that are characteristic of the PCET.

ACKNOWLEDGEMENTS

This work was supported in part by the National Natural Science Foundation of China under Grants No. 11775049 and No. 12375112. The Big Data Computing Center of Southeast University is acknowledged for providing the facility support for the partial numerical calculations of this work.

-
- [1] J.-R. Shen, *Annual review of plant biology* **66**, 23 (2015).
 - [2] D. J. Vinyard and G. W. Brudvig, *Annual review of physical chemistry* **68**, 101 (2017).
 - [3] Q.-F. Chen, Y.-H. Guo, Y.-H. Yu, and M.-T. Zhang, *Coordination Chemistry Reviews* **448**, 214164 (2021).
 - [4] M. Shamsipur and A. Pashabadi, *Coordination Chemistry Reviews* **374**, 153 (2018).
 - [5] C. F. Yocum, *Photosynthesis Research* **152**, 97 (2022).
 - [6] B. Kok, B. Forbush, and M. McGloin, *Photochemistry and Photobiology* **11**, 457 (1970).
 - [7] M. M. Najafpour, I. Zaharieva, Z. Zand, S. M. Hosseini, M. Kouzmanova, M. Holyńska, I. Tranca, A. W. Larkum, J.-R. Shen, and S. I. Allakhverdiev, *Coordination Chemistry Reviews* **409**, 213183 (2020).
 - [8] Y. Umena, K. Kawakami, J.-R. Shen, and N. Kamiya, *Nature* **473**, 55 (2011).

- [9] R. Pokhrel and G. W. Brudvig, *Physical Chemistry Chemical Physics* **16**, 11812 (2014).
- [10] N. Cox, M. Retegan, F. Neese, D. A. Pantazis, A. Bous-sac, and W. Lubitz, *Science* **345**, 804 (2014).
- [11] I. D. Young, M. Ibrahim, R. Chatterjee, S. Gul, F. D. Fuller, S. Koroidov, A. S. Brewster, R. Tran, R. Alonso-Mori, T. Kroll, *et al.*, *Nature* **540**, 453 (2016).
- [12] M. Suga, F. Akita, M. Sugahara, M. Kubo, Y. Nakajima, T. Nakane, K. Yamashita, Y. Umena, M. Nakabayashi, T. Yamane, *et al.*, *Nature* **543**, 131 (2017).
- [13] J. Kern, R. Chatterjee, I. D. Young, F. D. Fuller, L. Lassalle, M. Ibrahim, S. Gul, T. Fransson, A. S. Brewster, R. Alonso-Mori, *et al.*, *Nature* **563**, 421 (2018).
- [14] A. J. Wilson and P. K. Jain, *Journal of the American Chemical Society* **140**, 5853 (2018).
- [15] M. Ibrahim, T. Fransson, R. Chatterjee, M. H. Cheah, R. Hussein, L. Lassalle, K. D. Sutherlin, I. D. Young, F. D. Fuller, S. Gul, *et al.*, *Proceedings of the National Academy of Sciences* **117**, 12624 (2020).
- [16] R. Hussein, M. Ibrahim, A. Bhowmick, P. S. Simon, R. Chatterjee, L. Lassalle, M. Doyle, I. Bogacz, I.-S. Kim, M. H. Cheah, *et al.*, *Nature communications* **12**, 6531 (2021).
- [17] A. Bhowmick, R. Hussein, I. Bogacz, P. S. Simon, M. Ibrahim, R. Chatterjee, M. D. Doyle, M. H. Cheah, T. Fransson, P. Chernev, *et al.*, *Nature* **617**, 629 (2023).
- [18] P. Greife, M. Schönborn, M. Capone, R. Assunção, D. Narzi, L. Guidoni, and H. Dau, *Nature* **617**, 623 (2023).
- [19] A. P. Avramov, H. J. Hwang, and R. L. Burnap, *Proceedings of the National Academy of Sciences* **117**, 28036 (2020).
- [20] T. J. Wydrzynski, K. Satoh, and J. A. Freeman, *Photosystem II: the light-driven water: plastoquinone oxidoreductase*, Vol. 22 (Springer, 2005).
- [21] S. Styring, J. Sjöholm, and F. Mamedov, *Biochimica et Biophysica Acta (BBA)-Bioenergetics* **1817**, 76 (2012).
- [22] B. A. Barry and G. T. Babcock, *Proceedings of the National Academy of Sciences* **84**, 7099 (1987).
- [23] P.-Y. Huo, W.-Z. Jiang, R.-Y. Yang, and X.-R. Zhang, *Phys. Rev. Appl.* **21**, 024024 (2024).
- [24] T. Shimizu, M. Sugiura, and T. Noguchi, *The Journal of Physical Chemistry B* **122**, 9460 (2018).
- [25] H. Dau and M. Haumann, *Biochimica et Biophysica Acta (BBA)-Bioenergetics* **1767**, 472 (2007).
- [26] B. A. Barry, *Biochimica et Biophysica Acta (BBA)-Bioenergetics* **1847**, 46 (2015).
- [27] C. J. Gagliardi, A. K. Vannucci, J. J. Concepcion, Z. Chen, and T. J. Meyer, *Energy & Environmental Science* **5**, 7704 (2012).
- [28] G. Renger, *Biochimica et Biophysica Acta (BBA)-Bioenergetics* **1655**, 195 (2004).
- [29] I. Zaharieva, H. Dau, and M. Haumann, *Biochemistry* **55**, 6996 (2016).
- [30] S. Nakamura, M. Capone, D. Narzi, and L. Guidoni, *Physical Chemistry Chemical Physics* **22**, 273 (2020).
- [31] S. Nakamura, R. Nagao, R. Takahashi, and T. Noguchi, *Biochemistry* **53**, 3131 (2014).
- [32] D. Narzi, D. Bovi, and L. Guidoni, *Proceedings of the National Academy of Sciences* **111**, 8723 (2014).
- [33] K. Mittra and M. T. Green, *Journal of the American Chemical Society* **141**, 5504 (2019).
- [34] T. H. Yosca, J. Rittle, C. M. Krest, E. L. Onderko, A. Silakov, J. C. Calixto, R. K. Behan, and M. T. Green, *Science* **342**, 825 (2013).
- [35] R. Tyburski, T. Liu, S. D. Glover, and L. Hammarstrom, *Journal of the American Chemical Society* **143**, 560 (2021).
- [36] J. Stubbe, D. G. Nocera, C. S. Yee, and M. C. Chang, *Chemical reviews* **103**, 2167 (2003).
- [37] C. Aubert, M. H. Vos, P. Mathis, A. P. Eker, and K. Brettel, *Nature* **405**, 586 (2000).
- [38] M. N. Jackson, M. L. Pegis, and Y. Surendranath, *ACS central science* **5**, 831 (2019).
- [39] E. C. Minnihan, D. G. Nocera, and J. Stubbe, *Accounts of chemical research* **46**, 2524 (2013).
- [40] M. H. V. Huynh and T. J. Meyer, *Chemical Reviews* **107**, 5004 (2007).
- [41] J. W. Darcy, B. Koronkiewicz, G. A. Parada, and J. M. Mayer, *Accounts of chemical research* **51**, 2391 (2018).
- [42] Y. Tanabe and Y. Nishibayashi, *Angewandte Chemie*, e202406404.
- [43] Y. Ashida, Y. Onozuka, K. Arashiba, A. Konomi, H. Tanaka, S. Kuriyama, Y. Yamazaki, K. Yoshizawa, and Y. Nishibayashi, *Nature communications* **13**, 7263 (2022).
- [44] M. Esmaeilirad, Z. Jiang, A. M. Harzandi, A. Kondori, M. Tamadoni Saray, C. U. Segre, R. Shahbazian-Yassar, A. M. Rappe, and M. Asadi, *Nature Energy* **8**, 891 (2023).
- [45] F. Khezeli and C. Plaisance, *The Journal of Physical Chemistry A* **128**, 1576 (2024).
- [46] C. Costentin, *ACS Catalysis* **10**, 6716 (2020).
- [47] M. E. Tessensohn and R. D. Webster, *Current opinion in Electrochemistry* **15**, 27 (2019).
- [48] E. C. Gentry and R. R. Knowles, *Accounts of chemical research* **49**, 1546 (2016).
- [49] D. C. Miller, K. T. Tarantino, and R. R. Knowles, *Hydrogen Transfer Reactions: Reductions and Beyond*, 145 (2016).
- [50] P. R. Murray, J. H. Cox, N. D. Chiappini, C. B. Roos, E. A. McLoughlin, B. G. Hejna, S. T. Nguyen, H. H. Ripberger, J. M. Ganley, E. Tsui, *et al.*, *Chemical Reviews* **122**, 2017 (2021).
- [51] S. Hammes-Schiffer, *Accounts of Chemical Research* **42**, 1881 (2009).
- [52] D. G. Nocera, *Journal of the American Chemical Society* **144**, 1069 (2022).
- [53] P. Goyal and S. Hammes-Schiffer, *ACS Energy Letters* **2**, 512 (2017).
- [54] A. D. Becke, *The Journal of chemical physics* **96**, 2155 (1992).
- [55] C. Lee, W. Yang, and R. G. Parr, *Physical review B* **37**, 785 (1988).
- [56] S. H. Vosko, L. Wilk, and M. Nusair, *Canadian Journal of physics* **58**, 1200 (1980).
- [57] P. J. Stephens, F. J. Devlin, C. F. Chabalowski, and M. J. Frisch, *The Journal of physical chemistry* **98**, 11623 (1994).
- [58] Y. Guo, L. He, Y. Ding, L. Kloos, D. A. Pantazis, J. Messinger, and L. Sun, *Nature Communications* **15**, 5982 (2024).
- [59] V. Krewald, M. Retegan, F. Neese, W. Lubitz, D. A. Pantazis, and N. Cox, *Inorganic chemistry* **55**, 488 (2016).
- [60] M. Retegan, V. Krewald, F. Mamedov, F. Neese, W. Lubitz, N. Cox, and D. A. Pantazis, *Chemical Science* **7**, 72 (2016).

- [61] D. A. Horke, H. M. Watts, A. D. Smith, E. Jager, E. Springate, O. Alexander, C. Cacho, R. T. Chapman, and R. S. Minns, *Phys. Rev. Lett.* **117**, 163002 (2016).
- [62] W. Liu and H. H. Thorp, *Inorganic Chemistry* **32**, 4102 (1993).
- [63] R. Pal, C. F. Negre, L. Vogt, R. Pokhrel, M. Z. Ertem, G. W. Brudvig, and V. S. Batista, *Biochemistry* **52**, 7703 (2013).
- [64] P. E. Siegbahn, *Biochimica et Biophysica Acta (BBA)-Bioenergetics* **1827**, 1003 (2013).
- [65] D. Koulougliotis, D. J. Hirsh, and G. W. Brudvig, *Journal of the American Chemical Society* **114**, 8322 (1992).
- [66] M. Askerka, D. J. Vinyard, G. W. Brudvig, and V. S. Batista, *Biochemistry* **54**, 5783 (2015).
- [67] D. A. Pantazis, W. Ames, N. Cox, W. Lubitz, and F. Neese, *Angewandte Chemie International Edition* **51**, 9935 (2012).
- [68] J. Zimmermann and A. Rutherford, *Biochemistry* **25**, 4609 (1986).
- [69] A. Haddy, K. Lakshmi, G. W. Brudvig, and H. A. Frank, *Biophysical journal* **87**, 2885 (2004).
- [70] A. V. Astashkin, Y. Kodera, and A. Kawamori, *Journal of Magnetic Resonance, Series B* **105**, 113 (1994).